Inorg. Chem. **2007**, *46*, 8391–8402

Iron(III)–Catecholato Complexes as Structural and Functional Models of the Intradiol-Cleaving Catechol Dioxygenases

Pieter C. A. Bruijnincx,[†] Martin Lutz,[‡] Anthony L. Spek,*[,‡] Wilfred R. Hagen,*[,§] Gerard van Koten,[†] and Robertus J. M. Klein Gebbink*[,†]

Chemical Biology & Organic Chemistry, Faculty of Science, Utrecht University, Padualaan 8, 3584 CH Utrecht, The Netherlands, Bijvoet Center for Biomolecular Research, Crystal and Structural Chemistry, Faculty of Science, Utrecht University, Padualaan 8, 3584 CH Utrecht, The Netherlands, and Department of Biotechnology, Delft University of Technology, Julianalaan 67, 2628 BC Delft, The Netherlands

Received April 18, 2007

The structural and spectroscopic characterization of mononuclear iron(III)–catecholato complexes of ligand **L4** (methyl bis(1-methylimidazol-2-yl)(2-hydroxyphenyl)methyl ether, H**L4**) are described, which closely mimic the enzyme–substrate complex of the intradiol-cleaving catechol dioxygenases. The tridentate, tripodal monoanionic ligand framework of **L4** incorporates one phenolato and two imidazole donor groups and thus well reproduces the His_2Tyr endogenous donor set. In fact, regarding the structural features of $[Fe^{III}(\mathbf{L4})(tcc)(H_2O)]$ (**5**·H_2O, tcc = tetrachlorocatechol) in the solid state, the complex constitutes the closest structural model reported to date. The iron(III)–catecholato complexes mimic both the structural features of the active site and its spectroscopic characteristics. As part of its spectroscopic characterization, the electron paramagnetic resonance (EPR) spectra were successfully simulated using a simple model that accounts for *D* strain. The simulation procedure showed that the observed $g = 4.3$ line is an intrinsic part of the EPR envelope of the studied complexes and should not necessarily be attributed to a highly rhombic impurity. $[Fe^{III}(\mathbf{L4})(dtbc)(H_2O)]$ (dtbc = 3,5-di-*tert*-butylcatechol) was studied with respect to its dioxygen reactivity, and oxidative cleavage of the substrate was observed. Intradiol- and extradiol-type cleavage products were found in roughly equal amounts. This shows that an accurate structural model of the first-coordination sphere of the active site is not sufficient for obtaining regioselectivity.

Introduction

The oxidative cleavage of catechols is a key step in the biodegradation of aromatic compounds. In general, the responsible catechol dioxygenases can be divided into two classes, based on the position of the catechol ring cleavage (Figure 1).[1−4] The extradiol dioxygenases represent the more common metabolic pathway in which the C−C bond adjacent to the catechol oxygens is cleaved, whereas the intradiol dioxygenases cleave the C−C bond of the enediol functionality. The as-isolated state of the extradiol-cleaving enzymes is characterized by a non-heme iron(II) active site coordinated by the so-called 2-His-1-carboxylate facial triad, consisting of two histidines and one glutamate/aspartate residue.[5] On the other hand, the as-isolated intradiol dioxygenases show a non-heme iron(III) cofactor coordinated by two histidines, two tyrosines, and a hydroxide.[6,7] The active sites of the two types of enzymes are therefore quite distinct at first sight. However, upon substrate binding to the intradiol dioxyge-

* To whom correspondence should be addressed. E-mail: r.j.m.kleingebbink@chem.uu.nl (R.J.M.K.G.), w.r.hagen@tnw.tudelft.nl (W.R.H.), a.l.spek@chem.uu.nl (A.L.S., for correspondence pertaining to the crystallographic studies). Phone: +31-30-2531889 (R.J.M.K.G.), +31-15-2785051 (W.R.H.). Fax: +31-30-2523615 (R.J.M.K.G.), +31-15-2782355 (W.R.H.).

[†] Chemical Biology & Organic Chemistry, Utrecht University.

[‡] Bijvoet Center for Biomolecular Research, Utrecht University.

[§] Delft University of Technology.

(1) Bugg, T. D. H. *Tetrahedron* **2003**, *59*, 7075−7101.
(2) Bugg, T. D. H.; Lin, G. *Chem. Commun.* **2001**, 941−952.
(3) Costas, M.; Mehn, M. P.; Jensen, M. P.; Que, L., Jr. *Chem. Rev.* **2004**, *104*, 939−986.
(4) Solomon, E. I.; Brunold, T. C.; Davis, M. I.; Kernsley, J. N.; Lee, S-K.; Lehnert, N.; Neese, F.; Skulan, A. J.; Yang, Y-S.; Zhou, J. *Chem. Rev.* **2000**, *100*, 235−349.
(5) Koehntop, K. D.; Emerson, J. P.; Que, L., Jr. *J. Biol. Inorg. Chem.* **2005**, *10*, 87−93.
(6) Ohlendorf, D. H.; Lipscomb, J. D; Weber, P. C. *Nature* **1988**, *336*, 403−405.
(7) True, A. E.; Orville, A. M.; Pearce, L. L.; Lipscomb, J. D; Que, L., Jr. *Biochemistry* **1990**, *29*, 10847−10854.

10.1021/ic700741v CCC: $37.00
Published on Web 08/28/2007

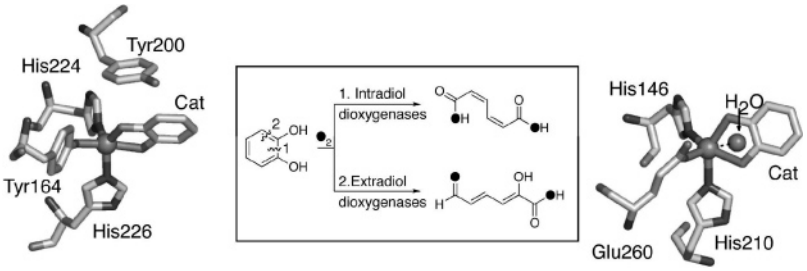

Figure 1. (center) Catechol cleavage by the intradiol- and extradiol-cleaving catechol dioxygenases. (left) Active-site structure of the enzyme−substrate complex of the intradiol-cleaving enzyme catechol 1,2-dioxygenase (1DLT). (right) Active-site structure of the enzyme−substrate complex of the extradiol-cleaving enzyme 2,3-dihydroxybiphenyl 1,2-dioxygenase (pdb 1KND).

nases, the axially coordinated tyrosine and the hydroxide ligand dissociate from the metal center.[8,9] The enzyme−substrate (E−S) complexes of both types of catechol dioxygenases, therefore, show an iron metal center coordinated by an N,N,O endogenous donor set (Figure 1), which differ in the type of the anionic donor (carboxylato vs phenolato) and the formal oxidation state of the metal.

In the extradiol-cleaving enzymes, substrate binding activates the ferrous center for the binding of dioxygen, whereas in the intradiol-cleaving enzymes, binding of the substrate to the ferric center is generally believed to activate the substrate itself toward direct reaction with dioxygen.[3,4] As an alternative for the latter mechanism, direct dioxygen binding to the metal has also been recently suggested on the basis of modeling[10,11] and theoretical studies[12,13] for the intradiol-cleaving enzymes. From this point on the respective mechanisms, however, all proceed through a similar bridged iron−alkylperoxo species. The different fates of this iron−alkylperoxo species then ultimately determine the outcome of the catechol cleavage for each class of enzymes.

Although much is known about each class of enzymes, the factors that determine the respective regioselectivities are yet to be fully understood. To better understand these underlying mechanisms, accurate biomimetic models can provide valuable insights. Many studies have been devoted to the modeling of the extra- and intradiol-cleaving enzymes, and impressive results have been obtained.[2,3,14] Since the enzymes utilize an ordered mechanism with substrate binding before dioxygen binding, isolated iron−catecholato complexes serve as a good starting point for these modeling studies. Many of the reported mimics of the catechol dioxygenases make use of tetradentate all-nitrogen donor ligands,[15−19] with probably the most well-studied system being the tris(2-pyridylmethyl)amine (tpa) complexes by Que et al.[20−22] Complexes with (several) phenolato groups in the ligand set have also been reported by various groups.[23−30] The ligands employed so far, however, do not accurately reflect the N_{im},N_{im},O_{phen}-ligand environment found at the active site of the enzymes (see Figure 1).

Recently, we described structural mimics of the E−S complex of the extradiol-cleaving dioxygenases.[31] The employed substituted bis(1-alkylimidazol-2-yl)propionate ligands **L1**−**L3**[32] accurately mimicked the 2-His-1-carboxylate facial triad found at the active site of these enzymes (Chart 1). Prompted by these results and the intriguing subtleties between the intra- and extradiol-cleaving enzymes, we set out to study the iron(III) coordination chemistry of **L4**[33] to mimic the active site of the intradiol-cleaving dioxygenases (Chart 1). Ligand **L4** includes the biologically relevant imidazole and phenolato donor groups in a tridentate, tripodal framework and is therefore an attractive candidate for the construction of an accurate model of the E−S complex. Although the ligand was first reported in the late

(8) Orville, A. M.; Lipscomb, J. D.; Ohlendorf, D. H. *Biochemistry* **1997**, *36*, 10052−10066.
(9) Vetting, M. W.; Ohlendorf, D. H. *Structure* **2000**, *8*, 429−440.
(10) Jo, D-H.; Que, L., Jr. *Angew. Chem., Int. Ed.* **2000**, *39*, 4284−4287.
(11) Hitomi, Y.; Tase, Y.; Higuchi, M.; Tanaka, T.; Funabiki, T. *Chem. Lett.* **2004**, *33*, 316−317.
(12) Borowski, T.; Siegbahn, P. E. M. *J. Am. Chem. Soc.* **2006**, *128*, 12941−12953.
(13) Funabiki, T.; Yamazaki, T. *J. Mol. Catal. A*: *Chem.* **1999**, *150*, 37−47.
(14) Yamahara, R.; Ogo, S.; Masuda, H.; Watanabe, Y. *J. Inorg. Biochem.* **2002**, *88*, 284−294.
(15) Hitomi, Y.; Yoshida, M.; Higuchi, M.; Minami, H.; Tanaka, T.; Funabiki, T. *J. Inorg. Biochem.* **2005**, *99*, 755−763.
(16) Merkel, M.; Pascaly, M.; Krebs, B.; Astner, J.; Foxon, S. P.; Schindler, S. *Inorg. Chem.* **2005**, *44*, 7582−7589.
(17) Mialane, P.; Tchertanov, L.; Banse, F.; Sainton, J.; Girerd, J.-J. *Inorg. Chem.* **2000**, *39*, 2440−2444.
(18) Pascaly, M.; Duda, M.; Schweppe, F.; Zurlinden, K.; Müller, F. K.; Krebs, B. *J. Chem. Soc., Dalton Trans.* **2001**, 828−837.
(19) Velusamy, M.; Mayilmurugan, R.; Palaniandavar, M. *J. Inorg. Biochem.* **2005**, *99*, 1032−1042.
(20) Cox, D. D.; Benkovic, S. J.; Bloom, L. M.; Bradley, F. C.; Nelson, M. J.; Que, L., Jr. *J. Am. Chem. Soc.* **1988**, *110*, 2026−2032.
(21) Cox, D. D.; Que, L., Jr. *J. Am. Chem. Soc.* **1988**, *110*, 8085−8092.
(22) Jang, H. G.; Cox, D. D.; Que, L., Jr. *J. Am. Chem. Soc.* **1991**, *113*, 9200−9204.
(23) Lauffer, R. B.; Heistand, R. H.; Que, L., Jr. *Inorg. Chem.* **1983**, *22*, 50−55.
(24) Merkel, M.; Müller, F. K.; Krebs, B. *Inorg. Chim. Acta* **2002**, *337*, 308−316.
(25) Ogo, S.; Yamahara, R.; Funabiki, T.; Masuda, H.; Watanabe, Y. *Chem. Lett.* **2001**, 1062−1063.
(26) Shongwe, M. S.; Kaschula, C. H.; Adsetts, M. S.; Ainscough, E. W.; Brodie, A. M.; Morris, M. J. *Inorg. Chem.* **2005**, *44*, 3070−3079.
(27) Velusamy, M.; Mayilmurugan, R.; Palaniandavar, M. *Inorg. Chem.* **2004**, *43*, 6284−6293.
(28) Velusamy, M.; Palaniandavar, M.; Gopalan, R. S.; Kulkarni, G. U. *Inorg. Chem.* **2003**, *42*, 8283−8293.
(29) Viswanathan, R.; Palaniandavar, M.; Balasubramanian, T.; Muthiah, T. P. *Inorg. Chem.* **1998**, *37*, 2943−2951.
(30) Yamahara, R.; Ogo, S.; Watanabe, Y.; Funabiki, T.; Jitsukawa, K.; Masuda, H.; Einaga, H. *Inorg. Chim. Acta* **2000**, *300*−*302*, 587−596.
(31) Bruijnincx, P. C. A.; Lutz, M.; Spek, A. L.; Hagen, W. R.; Weckhuysen, B. M.; van Koten, G.; Klein Gebbink, R. J. M. *J. Am. Chem. Soc.* **2007**, *129*, 2275−2286.
(32) Bruijnincx, P. C. A.; Lutz, M.; Spek, A. L.; van Faassen, E. L.; Weckhuysen, B. M.; van Koten, G.; Klein Gebbink, R. J. M. *Eur. J. Inorg. Chem.* **2005**, 779−787.
(33) Jameson, D. L.; Hilgen, S. E.; Hummel, C. E.; Pichla, S. L. *Tetrahedron Lett.* **1989**, *30*, 1609−1612.

Chart 1. Ligands **L1**−**L4**

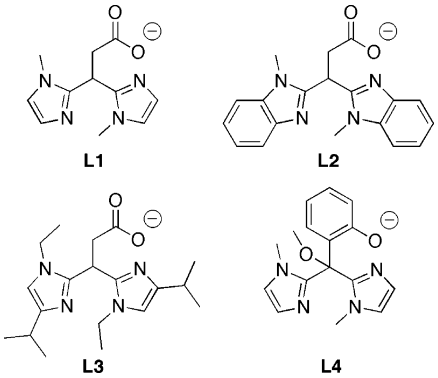

1980s by Jameson et al.,[33] to the best of our knowledge no metal complexes have been reported with **L4** to date.

Herein, we report on iron(III)−catecholato complexes of **L4**, representing the most accurate structural models of the E−S complexes of the intradiol enzymes to date. The synthesis and structural characterization of these complexes, as well as their dioxygen reactivity and product selectivity, is discussed.

Experimental Section

Air-sensitive organic reactions were carried out under an atmosphere of dry, oxygen-free N_2 using standard Schlenk techniques. Tetrachlorocatechol was recrystallized from anhydrous toluene before use. THF and hexanes were dried over sodium benzophenone ketyl and distilled under N_2 prior to use. Methanol was dried over magnesium methoxide and distilled under N_2 prior to use. All other chemicals were commercially obtained and used as received. The air-sensitive iron complex **6** was synthesized and handled under an argon atmosphere using standard Schlenk techniques. Solvents were thoroughly deoxygenated with argon before use. ^{1}H and ^{13}C NMR spectra were recorded on Varian AS400 or Varian Inova 300 spectrometers, operating at 25 °C. Elemental microanalyses were carried out by the Microanalytisches Laboratorium Dornis & Kolbe, Mulheim a.d. Ruhr, Germany. Electrospray ionization mass spectrometry (ESI-MS) spectra were recorded on a Micromass LC-TOF mass spectrometer by the Biomolecular Mass Spectrometry group, Utrecht University. Electron paramagnetic resonance (EPR) spectra were recorded on a Bruker ER 200 D spectrometer with an ER 4116 DM resonator and a home-built helium flow cooling system. UV−vis spectra were recorded on a Varian Cary 50 spectrometer equipped with a Helma emersion probe for air-sensitive experiments.

Methyl 2-Ethoxymethoxybenzoate (1). A solution of methyl salicylate (8.3 g, 54 mmol) in THF (30 mL) was added dropwise to a stirred suspension of NaH (8.6 g, 215 mmol, 60 wt % dispersion in mineral oil) in THF (500 mL). After stirring the resulting suspension for 1 h at room temperature, chloromethyl ethyl ether (10.2 g, 108 mmol) was added at once. The reaction mixture was then stirred overnight, filtered to remove the residual solid, and evaporated to dryness. The crude product was redissolved in hexanes (100 mL), dried over $MgSO_4$, filtered, and again evaporated to dryness. The resulting turbid oil was purified by flame distillation to yield the product as a colorless, clear oil (9.0 g, 79%). ^{1}H NMR (300 MHz, $CDCl_3$, 25 °C): δ = 1.17 (t, 3H, J = 6.9 Hz, OCH_2CH_3), 3.73 (q, 2H, J = 6.9 Hz OCH_2CH_3), 3.85 (s, 3H, OCH_3), 5.28 (s, 2H, OCH_2O), 6.99 (t, 1H, J = 6.0 Hz, H_{Ph}), 7.19 (d, 1H, J = 8.7 Hz, H_{Ph}), 7.40 (t, 1H, J = 6.6 Hz, H_{Ph}), 7.74 (d, 1H, J = 7.8 Hz, H_{Ph}). ^{13}C{^{1}H} (100 MHz, acetone-d_6, 25 °C): δ = 15.4, 52.1, 65.0, 94.5, 117.4, 122.1, 123.1, 131.6, 133.7, 157.3, 167.1.

Bis(1-methylimidazol-2-yl)(2-ethoxymethoxyphenyl)methanol (2). A solution of *n*-butyl lithium (24 mL, 38.4 mmol, 1.6 M solution in hexanes) was added dropwise to a solution of 1-methylimidazole (2.9 g, 35 mmol) and tetramethylethylenediamine (5 mL, 35 mmol) in THF (100 mL) at 0 °C. The solution was stirred for 1 h at 0 °C and subsequently cooled to −78 °C. A solution of **1** (3.5 g, 16.7 mmol) in THF (20 mL) was added dropwise to the stirred solution, and the reaction mixture was allowed to warm to room temperature overnight. The reaction mixture was quenched by the addition of 30 mL of a saturated aqueous NH_4Cl solution. All volatiles were evaporated in vacuo, and the aqueous layer was extracted with dichloromethane (4 × 50 mL). The combined organic extracts were dried over Na_2SO_4, filtered, and concentrated to dryness. The crude product was obtained as a brown oil and purified by column chromatography (silica, eluent ethyl acetate/triethylamine = 10:1). The product was obtained as a foamy, white solid (4.5 g, 79%). ^{1}H NMR (300 MHz, $CDCl_3$, 25 °C): δ = 1.13 (t, 3H, J = 7.2 Hz, OCH_2CH_3), 3.46 (q, 2H, J = 6.9 Hz, OCH_2CH_3), 3.53 (s, 6H, NCH_3), 5.09 (s, 2H, OCH_2O), 5.93 (s, 1H, O*H*), 6.43 (d, 1H, J = 7.7 Hz, H_{Ph}), 6.89 (s, 2H, H_{im}), 6.92 (t, 1H, J = 7.2 Hz, H_{Ph}), 6.96 (s, 2H, H_{im}), 7.20 (d, 1H, J = 8.4 Hz, H_{Ph}), 7.31 (t, 1H, J = 7.4 Hz, H_{Ph}). ^{13}C{^{1}H} (75 MHz, $CDCl_3$, 25 °C): δ = 15.2, 35.1, 64.6, 76.4, 93.9, 116.0, 122.1, 123.2, 126.5, 128.4, 130.3, 130.8, 148.1, 155.7.

Methyl Bis(1-methylimidazol-2-yl)(2-ethoxymethoxyphenyl)-methyl Ether (3). A solution of **2** (4.0 g, 11.7 mmol) in THF (30 mL) was added to a stirred suspension of NaH (1 g, 25 mmol, 60% weight dispersion in mineral oil) in THF (100 mL). The suspension was stirred for 1 h, after which MeI (2.0 g, 14 mmol) was added. The reaction mixture was stirred overnight at room temperature, quenched with a saturated, aqueous NH_4Cl solution (20 mL), diluted with H_2O (20 mL), and extracted with dichloromethane (3 × 50 mL). The combined organic extracts were dried over Na_2SO_4, filtered, and concentrated to dryness. The crude product was obtained as a yellowish-brown oil, which solidified upon standing. After purification by flash column chromatography (silica, first hexanes/Et_3N 10:1 v/v, then EtOAc/Et_3N 10:1 v/v), compound **3** was obtained as a white powder (2.9 g, 69%). ^{1}H NMR (300 MHz, $CDCl_3$, 25 °C): δ = 1.08 (t, 3H, J = 6.9 Hz, OCH_2CH_3), 3.29 (s, 3H, OCH_3), 3.42 (s, 6H, NCH_3), 3.43 (q, 2H, J = 6.3 Hz, OCH_2CH_3), 4.89 (s, 2H, OCH_2O), 6.82 (s, 2H, H_{im}), 6.96 (s, 2H, H_{im}), 6.99 (t, 1H, J = 7.7 Hz, H_{Ph}), 6.92 (t, 1H, J = 7.4 Hz, H_{Ph}), 7.27 (m, 2H, H_{Ph}). ^{13}C{^{1}H} (75 MHz, $CDCl_3$, 25 °C): δ = 15.2, 15.4, 34.7, 53.9, 64.0, 93.6, 116.0, 121.1, 123.0, 126.1, 126.8, 128.8, 130.4, 145.9, 156.5.

Methyl Bis(1-methylimidazol-2-yl)(2-hydroxyphenyl)methyl Ether (HL4). Compound **3** (2.4 g, 6.7 mmol) was dissolved in a mixture of methanol/hydrochloric acid (30%) (50 mL, 4:1 v/v), and the solution was refluxed for 1.5 h under N_2. The solution was allowed to cool to room temperature, and the methanol was evaporated in vacuo. The resulting aqueous solution was diluted (20 mL) and washed twice with pentane (2 × 20 mL). The pH of the aqueous solution was then adjusted to 8.2 by the addition of aqueous NaOH (1 M), and the solution was extracted with dichloromethane (3 × 40 mL). The organic layers were dried over Na_2SO_4, filtered, and evaporated in vacuo. The crude product was purified by column chromatography (silica, first EtOAc, then EtOAc/MeOH 5:1 v/v), and H**L4** was obtained as a white powder (1.4 g, 70%). Colorless, single crystals suitable for X-ray diffraction were obtained from an acetone solution cooled to −30 °C. ^{1}H NMR

(400 MHz, acetone-d_6, 25 °C): δ = 3.22 (s, 3H, OCH_3), 3.49 (s, 6H, NCH_3), 6.79 (d, 1H, J = 8.0 Hz, H_{Ph}), 6.85 (t, 1H, J = 7.4 Hz, H_{Ph}), 6.88 (s, 2H, H_{im}), 7.10 (s, 2H, H_{im}), 7.21 (m, 2H, H_{Ph}), 9.51 (s, 1H, OH). ^{13}C{^{1}H} (100 MHz, $CDCl_3$, 25 °C): δ = 34.7, 53.5, 81.5, 119.2, 119.8, 123.8, 124.2, 126.3, 127.0, 130.3, 145.3, 156.0. Anal. Calcd for $C_{16}H_{18}N_4O_2$ (298.34): C 64.41, H 6.08, N 18.78. Found: C 64.57, H 6.12, N 18.89. ESI-MS: m/z = 299.13 {[M + H]$^+$, calcd 299.15}, 321.08 {[M + Na]$^+$, calcd 321.13}.

[Fe(L4)$_2$](NO$_3$) (4). To a solution of H**L4** (159 mg, 0.53 mmol) and 1 equiv Et_3N (75 μL) in methanol (6 mL) was added an orange solution of $Fe(NO_3)_3$·$9H_2O$ (107 mg, 0.26 mmol) in methanol (6 mL), and immediately a color change to purple was observed. The solution was stirred for 20 min at 50 °C and concentrated in vacuo. The crude purple solid was redissolved in water (50 mL), and the product was extracted with dichloromethane (3 × 25 mL). The organic solution was washed twice with water (2 × 15 mL) and concentrated in vacuo. The crude product was then recrystallized from methanol/diethyl ether (1:2 v/v) at −30 °C to give the purple title compound (62 mg, 33% yield). Crystals suitable for X-ray diffraction were obtained by the slow evaporation of a methanolic solution of **4** at 4 °C. Anal. Calcd for $C_{32}H_{34}FeN_9O_7$ (712.51): C 53.94, H 4.81, N 17.69. Found: C 53.52, H 4.65, N 17.60. UV−vis (MeOH, ϵ (M^{-1} cm^{-1})): λ_{max} = 318 (5400), 540 (6400) nm. ESI-MS: m/z = 650.22 {[M − NO_3]$^+$, calcd 650.20}.

[Fe(L4)(tcc)] (5). To an orange solution of $Fe(NO_3)_3$·$9H_2O$ (220 mg, 0.54 mmol) in methanol (10 mL) was added a solution of H**L4** (162 mg, 0.54 mmol) and 1 equiv Et_3N (77 μL) in methanol (10 mL), and immediately a color change to dark blue was observed. The reaction mixture was stirred for 30 min at 50 °C. A solution of tetrachlorocatechol (H_2tcc) (135 mg, 0.54 mmol) and 2.2 equiv of Et_3N (170 μL) in methanol (10 mL) was added to the reaction mixture. The now purple reaction mixture was then stirred for 30 min at 50 °C, cooled to room temperature, and concentrated to 3 mL in vacuo. The crude product was precipitated with water, separated off, and washed with water (3 × 50 mL) and diethyl ether (2 × 50 mL). The product was obtained as a purple powder (245 mg, 76%) Crystals suitable for X-ray diffraction were obtained by the slow evaporation of a methanolic solution of **5** at room temperature. Anal. Calcd for $C_{22}H_{17}Cl_4FeN_4O_4$ (599.05): C 44.11, H 2.86, N 9.35. Found: C 43.88, H 3.00, N 9.67. UV−vis (MeOH, ϵ (M^{-1} cm^{-1})): λ_{max} = 303 (8500), 560 (4000) nm. ESI-MS: m/z = 599.85 {[M + H]$^+$, calcd 599.94}.

[Fe(L4)(dtbc)] (6). To an orange solution of $Fe(NO_3)_3$·$9H_2O$ (304 mg, 0.75 mmol) in methanol (15 mL) was added a solution of H**L4** (224 mg, 0.75 mmol) and 1 equiv Et_3N (110 μL) in methanol (20 mL), and immediately a color change was observed to dark blue. The reaction mixture was stirred for 20 min at 50 °C. A solution of 3,5-di-*tert*-butylcatechol (H_2dtbc) (168 mg, 0.75 mmol) and 2.2 equiv of Et_3N (230 μL) in methanol (10 mL) was added to the reaction mixture. The purple reaction mixture was then stirred for 20 min at 50 °C, cooled to room temperature, and concentrated to 2 mL in vacuo. The crude product was precipitated with water, separated off, and washed with water (3 × 50 mL) and hexanes (2 × 50 mL). The product was obtained as a purple-black powder (410 mg, 95%). Anal. Calcd for $C_{30}H_{37}FeN_4O_4$ (573.48): C 62.83, H 6.50, N 9.77. Found: C 62.75, H 6.71, N 9.58. UV−vis (MeOH, ϵ (M^{-1} cm^{-1})): λ_{max} = 316 (5400), 524 (4000), 720 (sh, 2500) nm. ESI-MS: m/z = 573.14 {[M]$^+$, calcd 573.22}.

Oxygenation Reactions and Characterization of Oxygenation Products. In a typical reaction, 25 mg of [Fe^{III}(**L4**)(dtbc)] (**6**) was dissolved in 40 mL of solvent and the purple solution was exposed to air and stirred for two weeks after which 1 equiv of internal standard (1,3,5-tribromobenzene) was added to the solution. The solvent was then removed in vacuo, and the residue was redissolved in 10 mL of DMF and 25 mL of 4 M HCl was added to decompose the metal complexes. The resulting solution was extracted with chloroform (3 × 20 mL). The combined organic layers were washed with 1 M HCl (20 mL) and water (20 mL), dried over $MgSO_4$, filtered, and evaporated in vacuo. The products were analyzed by GC-MS and ^{1}H NMR. The combined intradiol, extradiol, and quinone products accounted for at least >85% of the converted dtbc reactant. The quinone auto-oxidation product could not be accurately detected by GC-MS, and the products were therefore quantified by ^{1}H NMR. Authentic samples of the intradiol products 3,5-di-*tert*-butyl-1-oxacyclohepta-3,5-diene-2,7-dione and 3,5-di-*tert*-butyl-5-carboxymethyl-2-furanone methyl ester were prepared according to a published procedure.[34] Authentic samples of the extradiol product isomers 3,5-di-*tert*-butyl-2-pyrone and 4,6-di-*tert*-butyl-2-pyrone were prepared by reacting [FeCl(dtbc)(Me_3-tacn)] with air as described by Que et al.[10]

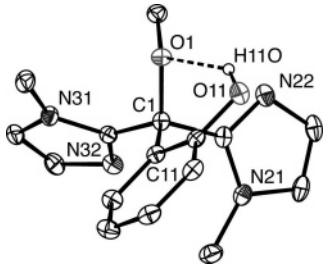

Figure 2. Molecular structure of H**L4** in the crystal with the intramolecular hydrogen bond between H11O and O1. All C−H hydrogen atoms have been omitted for clarity. Displacement ellipsoids are drawn at the 30% probability level. Hydrogen bond lengths and angles for H**L4**: O11−H11O···O1, D−H = 0.91(4) Å, H···A 1.94(4) Å, D···A = 2.704(3) Å, D−H···A = 141(3)° (D, hydrogen bond donor atom; A, hydrogen bond acceptor atom).

X-ray Crystal Structure Determinations of HL4, 4, and 5·H$_2$O. X-ray intensities were measured on a Nonius KappaCCD diffractometer with rotating anode and graphite monochromator (λ = 0.71073 Å) at a temperature of 150 K. The structures were solved with direct methods (*SHELXS-97*[35] for H**L4**, *SIR2004*[36] for **4**, and *SIR97*[37] for **5**·H_2O) and refined with *SHELXL-97*[38] against F^2 of all reflections. Geometry calculations and checking for higher symmetry were performed with the *PLATON*[39] program. H**L4** consisted of two crystal fragments, of which the intensities were integrated separately with the program *EvalCCD*.[40] Refinement was performed using a HKLF5 file.[41] All hydrogen atoms were located in the difference Fourier map. The OH hydrogen atom was refined freely with isotropic displacement parameters. All other hydrogen atoms were refined with a riding model. In **4**, all hydrogen atoms were located in the difference Fourier map and were refined with a riding model. In **5**·H_2O, all hydrogen atoms were located in the difference Fourier map. The OH hydrogen atoms were refined freely

(34) Demmin, T. R.; Rogic, M. M. *J. Org. Chem.* **1980**, *45*, 1153−1156.
(35) Sheldrick, G. M. *SHELXS-97, Program for Crystal Structure Solution*; University of Göttingen: Göttingen, Germany, 1997.
(36) Burla, M. C.; Caliandro, R.; Camalli, M.; Carrozzini, B.; Cascarano, G. L.; De Caro, L.; Giacovazzo, C.; Polidori, G.; Spagna, R. *J. Appl. Crystallogr.* **2005**, *38*, 381−388.
(37) Altomare, A.; Burla, M. C.; Camalli, M.; Cascarano, G. L.; Giacovazzo, C.; Guagliardi, A.; Moliterni, A. G. G.; Polidori, G.; Spagna, R. *J. Appl. Crystallogr.* **1999**, *32*, 115−119.
(38) Sheldrick, G. M. *SHELXL-97, Program for Crystal Structure Refinement*; University of Göttingen: Göttingen, Germany, 1997.
(39) Spek, A. L. *J. Appl. Crystallogr.* **2003**, *36*, 7−13.
(40) Duisenberg, A. J. M.; Kroon-Batenburg, L. M. J.; Schreurs, A. M. M. *J. Appl. Crystallogr.* **2003**, *36*, 220−229.
(41) Herbst-Irmer, R.; Sheldrick, G. M. *Acta Crystallogr.* **1998**, *B54*, 443−449.

Table 1. Crystallographic Data for Compounds H**L4**, **4**, and **5**·H_2O

	H**L4**	**4**	**5**·H_2O
formula	$C_{16}H_{18}N_4O_2$	$[C_{32}H_{34}FeN_8O_4](NO_3)$	$C_{22}H_{19}Cl_4FeN_4O_5$
fw	298.34	712.53	617.06
cryst color	colorless	dark purple	black
cryst size [mm^3]	0.09 × 0.09 × 0.09	0.33 × 0.10 × 0.06	0.12 × 0.12 × 0.06
cryst syst	triclinic	monoclinic	triclinic
space group	$P\bar{1}$ (No. 2)	$P2_1/c$ (No. 14)	$P\bar{1}$ (No. 2)
A [Å]	8.6380(4)	13.9987(1)	9.4907(3)
b [Å]	8.8289(5)	12.2216(1)	10.8082(4)
c [Å]	10.9157(8)	19.6864(2)	13.2111(5)
α [deg]	80.941(2)		106.1042(13)
β [deg]	72.880(3)	101.9129(4)	102.8529(12)
γ [deg]	67.299(3)		101.8027(13)
V [$Å^3$]	733.05(8)	3295.54(5)	1217.00(8)
Z	2	4	2
D_x [g/cm^3]	1.352	1.436	1.684
μ [mm^{-1}]	0.092	0.520	1.102
abs corr method		multiscan	multiscan
abs corr range		0.91−0.97	0.83−0.94
$(\sin\theta/\lambda)_{max}$ [$Å^{-1}$]	0.61	0.65	0.60
reflns (measd/unique)	7642/2722	73042/7533	15576/4292
params/restraints	207/0	448/0	336/0
R1/wR2 [$I > 2\sigma(I)$]	0.0629/0.1409	0.0372/0.0905	0.0414/0.1026
R1/wR2 [all reflns]	0.1008/0.1646	0.0616/0.1007	0.0657/0.1163
S	1.081	1.091	1.068
$\rho_{min/max}$ [$e/Å^3$]	−0.32/0.31	−0.53/0.38	−0.38/0.40

Scheme 1. Synthesis of H**L4**

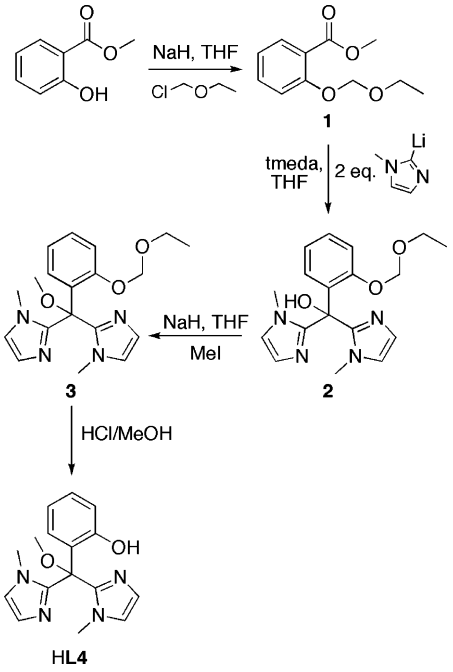

with isotropic displacement parameters. All other hydrogen atoms were refined with a riding model. Further crystallographic details are given in Table 1.

Results

Synthesis of Ligand HL4. Ligand H**L4** was synthesized through an adapted literature procedure.[33] H**L4** can be conveniently synthesized on a multigram scale from methyl salicylate in four steps (Scheme 1). The hydroxyl group of methyl salicylate was protected with an ethoxymethyl ether (79% yield), and the resulting ester **1** was reacted with 2 equiv of 2-lithio-1-methylimidazole in THF at −78 °C to yield **2** in 79% yield after column chromatography. The hydroxyl group of **2** was then converted into the methoxy ether **3** with NaH and iodomethane (69%) to prevent any ambiguity in the potential donor set of the ligand.[33] In the last step, the ethoxymethyl ether protecting group of **3** was cleaved and H**L4** was obtained as a white powder after column chromatography in 70% yield.

The molecular structure of H**L4** was confirmed by single-crystal X-ray diffraction (Figure 2). Suitable crystals of H**L4** grew upon standing from a saturated acetone solution at −30 °C. Interestingly, the phenolic OH group is *intra*molecularly hydrogen bonded to the methoxy oxygen atom O1. This hydrogen bond effectively locks the phenol donor group in a fixed position, at least in the solid state. The hydrogen-bonded hydroxyl group is readily observed in the IR absorption spectrum of solid H**L4** as a sharp and intense absorption band at 3351 cm^{-1}. It is also manifested in solution, since a sharp singlet at 9.51 ppm is observed for the hydroxyl proton in the ^1H NMR spectrum of H**L4** recorded in acetone-d_6.

Synthesis of Iron(III) Complexes. To investigate the facial-capping potential of **L4**, we first synthesized the 2:1 complex of **L4** with an Fe^{III} metal center (Chart 2). The addition of a methanolic solution of $^1/_2$ equiv of $Fe(NO_3)_3$·$9H_2O$ to a solution containing equimolar amounts of H**L4** and Et_3N in methanol resulted in the immediate formation of the deep purple product, which was identified as $[Fe^{III}(\mathbf{L4})_2](NO_3)$ (**4**).

Iron(III)−catecholato complexes of ligand **L4** with two different catechols, i.e., tetrachlorocatechol (H_2tcc) and 3,5-di-*tert*-butylcatechol (H_2dtbc), were also prepared. The complexes $[Fe^{III}(\mathbf{L4})(tcc)]$ (**5**) and $[Fe^{III}(\mathbf{L4})(dtbc)]$ (**6**) were synthesized by the addition of a methanolic solution of $Fe(NO_3)_3$·$9H_2O$ to a methanolic solution containing equimolar amounts of H**L4** and Et_3N. The reaction mixture immediately turned deep blue and was stirred at elevated temperatures to ensure full chelation of the ligand through all donor atoms

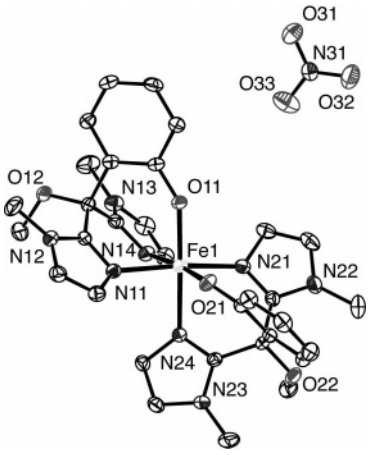

Figure 3. Molecular structure of **4** in the crystal. All hydrogen atoms have been omitted for clarity. Displacement ellipsoids are drawn at the 50% probability level.

Chart 2. Iron(III) Complexes of **L4**

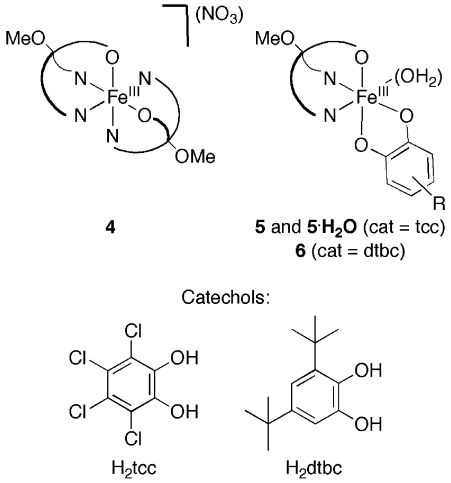

(vide infra). Subsequent addition of a solution of the appropriate catechol and 2 equiv of Et_3N resulted in a direct color change to deep purple. Both the air-stable complex **5** and the air-sensitive complex **6** were isolated in good yields as purple powders. The iron(III) complexes **5** and **6** were obtained as neutral, five-coordinate complexes, in which the monoanionic, tridentate ligand and a dianionic, chelated catecholato ligand carry the negative charges. It is important to note at this point that the complexes **5** and **6** are obtained solvent-free, according to elemental analysis. The five-coordinate iron(III) complexes can bind an additional ligand such as water (vide infra) or other coordinating solvents. The structures of **4** and **5**·H_2O were established by X-ray crystal-structure determination.

Crystal Structure of 4. Purple crystals suitable for X-ray diffraction were obtained by the slow evaporation of a methanolic solution of **4** at 4 °C. The molecular structure of **4** is shown in Figure 3, with selected bond lengths and angles presented in Table 2.

Two monoanionic **L4** ligands facially cap the iron(III) center in **4** through both 1-methylimidazole groups and the phenolato group, resulting in a six-coordinate iron(III) center with a N_4O_2 donor set. The two ligands are not arranged centrosymmetrically around the iron ion, but rather are rotated by 120° relative to each other. This results in a cis dispositioning of the phenolato O-donor atoms, each located trans to a 1-methylimidazole group. This cis disposition of the phenolato groups has also been observed in related complexes,[42−46] e.g., in $[Fe^{III}(L)_2](ClO_4)$·MeCN with the facially coordinated (2-hydroxyphenyl)bis(pyrazolyl)methane ligand.[44] The Fe−N bond lengths Fe1−N14 and Fe1−N24 (2.1323 and 2.1378 Å, respectively) are longer than the other two Fe−N bond lengths, which can be attributed to the positioning of the strong phenolato donors positioned trans to N14 and N24. The average Fe−O and Fe−N bond lengths are in accordance with the values for related Fe(III) complexes with an N_4O_2 donor set.[42−46] The geometry of **4** is distorted octahedral with the phenolato oxygens (O11 and O21) and imidazole nitrogens N14 and N24 occupying the equatorial plane. The diminished angles found for N14−Fe1−N11 and N24−Fe1−N21 (82.15(6) and 83.24(6)°) deviate quite strongly from ideal octahedral geometry and are dictated by the inherent geometrical restrictions imposed by the tripodal ligand.

Table 2. Selected Bond Lengths (Å) and Angles (deg) for **4**

	bond length		angle		angle
Fe1−N11	2.1014(15)	O11−Fe1−N24	174.08(6)	O11−Fe1−N14	87.74(6)
Fe1−N14	2.1323(16)	O21−Fe1−N14	174.12(6)	N14−Fe1−N24	86.58(6)
Fe1−N21	2.0812(16)	N11−Fe1−N21	171.08(6)	N24−Fe1−O21	87.86(6)
Fe1−N24	2.1378(15)			O21−Fe1−O11	97.87(6)
Fe1−O11	1.9104(13)	N14−Fe1−N11	82.15(6)	N11−Fe1−N24	90.15(6)
Fe1−O21	1.9077(12)	N11−Fe1−O21	95.95(6)	N24−Fe1−N21	83.24(6)
		O21−Fe1−N21	89.80(6)	N21−Fe1−O11	95.22(6)
		N21−Fe1−N14	91.46(6)	O11−Fe1−N11	90.75(6)

Crystal Structure of 5·H_2O. Blue-purple crystals of **5**·H_2O suitable for X-ray diffraction were obtained by the slow evaporation of a methanolic solution of **5** under ambient conditions. Upon crystallization, the complex picked up a water molecule from the (wet) solvent and a six-coordinate iron complex was obtained. The molecular structure of **5**·H_2O is depicted in Figure 4, with selected bond lengths and angles presented in Table 3.

The iron(III) metal center in **5**·H_2O is facially capped by the three donor atoms of the N,N,O-coordinated ligand. A chelated tetrachlorocatecholato ligand and a water molecule complete the distorted-octahedral coordination sphere. The crystal structure of **5**·H_2O very closely resembles the structure found for [Fe(**L3**)(tcc)(H_2O)] (**L3** = 3,3-bis(1-ethyl-4-isopropylimidazol-2-yl)propionate), which we recently reported as a close structural mimic of the extradiol-cleaving catechol dioxygenases.[31] The two complexes differ in the oxygen donor atom of the N,N,O-donor set offered by the ligand, i.e., a phenolato O in **L4** vs a carboxylato O in **L3**.

(42) Davis, J. C.; Kung, W.-J.; Averill, B. A. *Inorg. Chem.* **1986**, *25*, 394−396.
(43) Hayami, S.; Gu, Z.-Z.; Shiro, M.; Einaga, Y.; Fujishima, A.; Sato, O. *J. Am. Chem. Soc.* **2000**, *122*, 7126−7127.
(44) Higgs, T. C.; Ji, D.; Czernuscewicz, R. S.; Carrano, C. J. *Inorg. Chim. Acta* **1999**, *286*, 80−92.
(45) Lubben, M.; Meetsma, A.; van Bolhuis, F.; Feringa, B. L.; Hage, R. *Inorg. Chim. Acta* **1994**, *215*, 123−129.
(46) Imbert, C.; Hratchian, H. P.; Lanznaster, M.; Heeg, M. J.; Hryhorczuk, L. M.; McGarvey, B. R.; Schlegel, H. B.; Verani, C. N. *Inorg. Chem.* **2005**, *44*, 7414−7422.

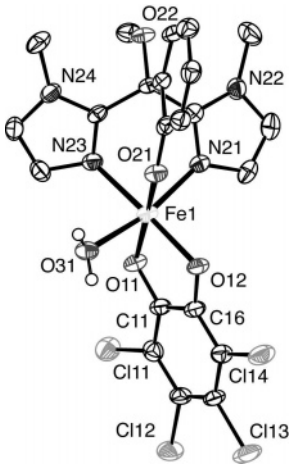

Figure 4. Molecular structure of **5**·H_2O in the crystal. All C−H hydrogen atoms have been omitted for clarity. Displacement ellipsoids are drawn at the 50% probability level.

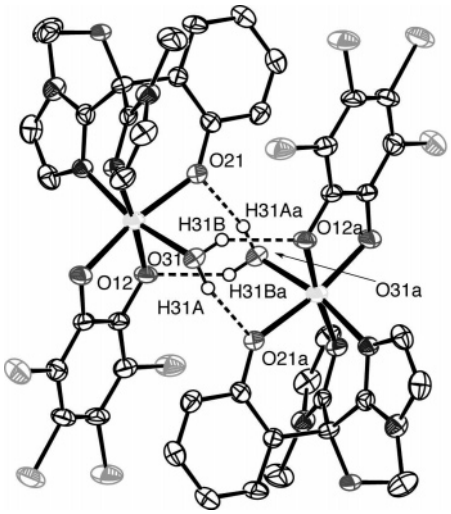

Figure 5. Hydrogen-bonding pattern in **5**·H_2O. All C−H hydrogen atoms have been omitted for clarity. Symmetry operation a: $1 - x, 1 - y, 1 - z$.

The tetrachlorocatecholato ligand in **5**·H_2O is coordinated trans to the phenolato group and one of the imidazoles. The Fe1−O21 phenolato bond length (2.006(2) Å) is significantly longer than the Fe−O phenolato bond length found in **4** (average Fe−O 1.909 Å). This is probably caused by both the different trans influences exerted by an imidazole N and a catecholato O, respectively, and the involvement of the phenolato oxygen in a hydrogen bonding interaction in **5**·H_2O (vide infra).

Only a few crystal structures of iron(III)−catecholato complexes with a phenolate-containing ligand system have been reported to date, of which only one contains a tridentate ligand with an N,N,O_{phen}-donor set.[23−25,30] The Fe−O_{phen} bond length found in **5**·H_2O is comparable to those reported for the complexes [Fe(L)(tbc)][24] (L = substituted bis(2-hydroxybenzyl)(2-pyridylmethyl)amines) (average Fe−O_{phen} length 2.001 Å) and [Fe(salen)(cat)] (1.989 Å),[23] but longer than those observed in [Fe(L)Cl(dtbc)][25] (L = *N*-(2-hydroxyphenyl)-*N*-(2-pyridylmethyl)benzylamine) (1.957 Å) and [Fe(L)(dtbc)][30] (L, (2-hydroxyphenyl)-bis(pyridylmethyl)amine) (1.953 Å). The Fe1−N21 and Fe1−N23 bond lengths differ slightly (2.089(3) Å vs 2.119(3) Å) and are somewhat shorter than the Fe−N bond lengths in [Fe(**L3**)(tcc)(H_2O)].[31]

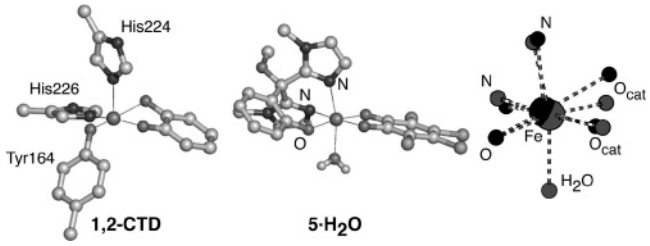

Figure 6. First coordination sphere of the iron(III) metal center of the catechol 1,2-dioxygenase E−S complex (1,2-CTD, pdb 1DLT) (left) and that of complex **5**·H_2O (middle). Quaternion fit[39] (right) of the iron(III) metal center and the donor atoms in the enzyme−substrate complex (black) and the donor atoms in **5**·H_2O (gray) (The gray sphere of the phenolato donor atom of the model complex is obscured due to exact overlap).

The catecholato ligand is bound symmetrically to the iron center with essentially equal Fe−O bond lengths (Fe1−O11 = 1.967(2) Å and Fe1−O12 = 1.973(2) Å). This is rather unexpected, given the different donor groups located trans to each of the catechol oxygens. The binding of dianionic catecholates trans to different donor groups has been reported to lead to asymmetric chelation with the strongest interaction trans to the weaker donor group.[18,21,47] The symmetric binding of the catechol in **5**·H_2O can be the consequence of the involvement of both phenolato oxygen O21 and catecholato oxygen O12 in hydrogen bonding interactions. In fact, the water molecule is engaged in two hydrogen bonds with a second complex, resulting in the formation of centrosymmetric dimers of **5**·H_2O in the solid state (Figure 5 and Table 4); hydrogen atom H31A is bonded intermolecularly to phenolato O21, while hydrogen atom H31B is bonded intermolecularly to catecholato oxygen O12. The first interaction weakens the donor strength of O21, while the second weakens the interaction of catecholato oxygen O12 with the metal center. This results, in this particular case, in equal Fe−O_{cat} bond lengths.

A similar hydrogen-bonding pattern and formation of dimers in the solid state was observed for the closely related [Fe(**L3**)(tcc)(H_2O)].[31] In [Fe(**L3**)(tcc)(H_2O)], the effects of the hydrogen bonding on the iron−catecholato bond lengths are more pronounced, resulting in an asymmetric binding mode of the catechol. The C11−O11 and C16−O12 bond lengths in the tcc moiety in **5**·H_2O are similar (1.331(4) and 1.344(4) Å, respectively) and are comparable to those found in the other Fe(III)−tetrachlorocatecholato complexes.[16,18,48] Together with the regular C−C bond lengths of the aromatic ring, it is clear that the catecholato ligand is bound as a O,O dianion. No structural evidence for the manifestation of partial semiquinone character of the catecholato ligand is found.[49]

The geometry of **5**·H_2O can be best described as a severely distorted octahedron with the catecholato oxygens (O11 and

(47) Jo, D-H.; Chiou, Y-M.; Que, L., Jr. *Inorg. Chem.* **2001**, *40*, 3181−3190.
(48) Merkel, M.; Schnieders, D.; Baldeau, S. M.; Krebs, B. *Eur. J. Inorg. Chem.* **2004**, 783−790.
(49) Mialane, P.; Anxolabéhère-Mallart, E.; Blondin, G.; Nivorojkine, A.; Guilhem, J.; Tchertanova, L.; Cesario, M.; Ravi, N.; Bominaar, E.; Girerd, J.-J.; Münck, E. *Inorg. Chim. Acta* **1997**, *263*, 367−378.

Table 3. Selected Bond Lengths (Å) and Angles (deg) for **5**·H_2O

bond length			angle		angle
Fe1−N21	2.089(3)	O12−Fe1−N23	174.23(10)	O31−Fe1−N23	89.12(10)
Fe1−N23	2.119(3)	O21−Fe1−O11	171.20(9)	N23−Fe1−N21	82.75(10)
Fe1−O21	2.006(2)	O31−Fe1−N21	167.74(11)	N21−Fe1−O12	96.92(10)
Fe1−O11	1.967(2)			O12−Fe1−O31	92.08(10)
Fe1−O12	1.973(2)				
Fe1−O31	2.127(3)	O21−Fe1−O31	83.91(10)	N23−Fe1−O21	92.94(10)
C11−O11	1.331(4)	O31−Fe1−O11	88.64(10)	O21−Fe1−O12	92.79(9)
C16−O12	1.344(4)	O11−Fe1−N21	100.71(10)	O12−Fe1−O11	82.79(9)
		N21−Fe1−O21	87.34(9)	O11−Fe1−N23	91.61(10)

Table 4. Selected Hydrogen Bond Lengths (Å) and Angles (deg) for **5**·H_2O[a]

donor−H···acceptor	D−H	H···A	D···A	D−H···A
O31−H31A···O21a	0.83(5)	1.95(5)	2.748(3)	160(5)
O31−H31B···O12a	0.81(4)	2.07(4)	2.759(3)	143(3)

[a] Symmetry operation a: $1 - x, 1 - y, 1 - z$.

O12), imidazole N23, and phenolato O21 occupying the equatorial plane. The axial positions are occupied by imidazole N21 and the water molecule. The angular deviation from ideal octahedral geometry is caused by inherent geometrical restrictions imposed by the tripodal ligand and the involvement of the water molecule in two moderately strong hydrogen bonds.

Structural Comparison with the Intradiol-Cleaving Enzymes. Crystal structure information is available for several intradiol-cleaving catechol dioxygenases. The structures of the as-isolated states of four different intradiol-cleaving enzymes have been reported.[6,50−53] In addition, the crystal structures of enzyme−substrate complexes of the enzymes protocatechuate 3,4-dioxygenase from *Pseudonomas putida* (3,4-PCD) and catechol 1,2-dioxygenase from *Acinetobacter calcoaceticus* ADP1 (1,2-CTD) with different catechols are known.[8,9,54] Prior to substrate binding, the ferric ion at the active site is coordinated by four endogenous ligands, i.e., two tyrosines and two histidines and a hydroxide resulting in a trigonal-bipyrimidal geometry. Substrate binding results in the displacement of both the hydroxide ligand and the axial tyrosine residue. The active-site geometry of the enzyme−substrates complexes can, therefore, best be described as octahedral with one open coordination site.[9] At this stage the pentacoordinate ferric metal center is coordinated by only three endogenous ligands (His_2Tyr) and an asymmetrically bound catecholato dianion.[55] A comparison of the active-site structure of 1,2-CTD and the structure of complex **5**·H_2O is shown in Figure 6.

From this comparison, **5**·H_2O can be regarded as a close structural mimic of the enzyme−substrate (E−S) complex of the intradiol-cleaving catechol dioxygenases. Ligand **L4** accurately models the endogenous donor groups of the enzyme. The trans disposition of the ligands is the same in the E−S complex and in the model compound. In both cases, the catechol is coordinated trans to one of the imidazoles and the phenolato moiety. The sixth coordination site is located in both structures trans to an imidazole group and is open in the E−S complex and occupied by a water molecule in **5**·H_2O. The availability of this vacant site is important for the formation of an implicated bridged alkylperoxo intermediate (vide infra). In the crystal structure of 3,4-PCD·INO, with the substrate analogue 2-hydroxyisonicotinic acid *N*-oxide (INO), the sixth coordination site is also occupied by a water molecule.[8] The $Fe-O_{cat}$ bond lengths differ significantly (~0.3 Å) in the enzyme but are almost equal in the model complex. The asymmetric chelation in the enzyme−substrate complex is attributed to the different trans influences exerted by the histidine and tyrosine residues and the involvement of one of the catecholato oxygens in a hydrogen bond.[3,55] Both factors also play a role in complex **5**·H_2O, but now the hydrogen bonding interactions counterbalance the effect of the different trans ligands. All these features are illustrated by a quaternion fit[39] of the donor atoms and the metal center of both the E−S complex and the model compound (Figure 6, right).

Electronic Absorption and EPR Spectra. Two important features of the UV−vis absorption spectrum of **4** in methanol are the absorption bands at 318 ($\epsilon = 6400\ M^{-1}\ cm^{-1}$) and 540 nm ($\epsilon = 6400\ M^{-1}\ cm^{-1}$), of which the latter gives rise to the typical purple color of the complex (Figure 7).

These bands can both be assigned to phenolato-to-iron(III) charge-transfer transitions from the p_π to the d_σ* and d_π* orbitals of the Fe(III) ion, respectively.[46,56] The absorptions are slightly blue-shifted compared with the related $[Fe^{III}(L)_2](ClO_4)$ (L = (2-hydroxyphenol)bis(pyrazolyl) methane; λ_{max} = 324 and 570 nm).[44] This shift to higher energy is correlated to the longer iron−phenolato distance (1.91 vs 1.88 Å) and, consequently, the weaker phenolato-to-iron overlap. The absorption feature at 285 nm, which is observed for all complexes, is ligand-based and can probably be assigned to a $\pi \rightarrow \pi^*$ transition involving the phenolato moiety.

The electronic spectra of **5** and **6** both show a much broader absorption feature in the visible region. Compound

(50) Ferraroni, M.; Seifert, J.; Travkin, V. M.; Thiel, M.; Kaschabek, S.; Scozzafava, A.; Golovleva, L.; Schlömann, M.; Briganti, F. *J. Biol. Chem.* **2005**, *280*, 21133−21154.
(51) Ferraroni, M.; Solyanikova, I. P.; Kolomytseva, M. P.; Scozzafava, A.; Golovleva, L.; Briganti, F. *J. Biol. Chem.* **2004**, *279*, 27646−27655.
(52) Ohlendorf, D. H.; Orville, A. M.; Lipscomb, J. D. *J. Mol. Biol.* **1994**, *244*, 586−608.
(53) Vetting, M. W.; D'Argenio, D. A.; Ornston, L. N.; Ohlendorf, D. H. *Biochemistry* **2000**, *39*, 7943−7955.
(54) Elgren, T. E.; Orville, A. M.; Kelly, K. A.; Lipscomb, J. D.; Ohlendorf, D. H.; Que, L., Jr. *Biochemistry* **1997**, *36*, 11504−11513.
(55) Horsman, G. P.; Jirasek, A.; Vaillancourt, F. H.; Barbosa, C. J.; Jarzecki, A. A.; Xu, C.; Mekmouche, Y.; Spiro, T. G.; Lipscomb, J. D.; Blades, M. W.; Turner, R. F. B.; Eltis, L. D. *J. Am. Chem. Soc.* **2005**, *127*, 16882−16891.
(56) Gaber, B. P.; Miskowski, V.; Spiro, T. G. *J. Am. Chem. Soc.* **1974**, *96*, 6868−6873.

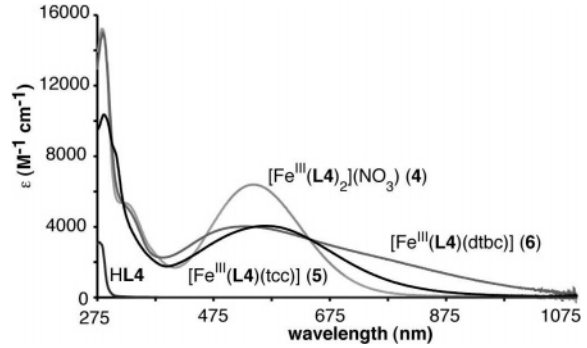

Figure 7. UV−vis absorption spectra of **4**−**6** and H**L4**. All spectra were recorded in methanol solution.

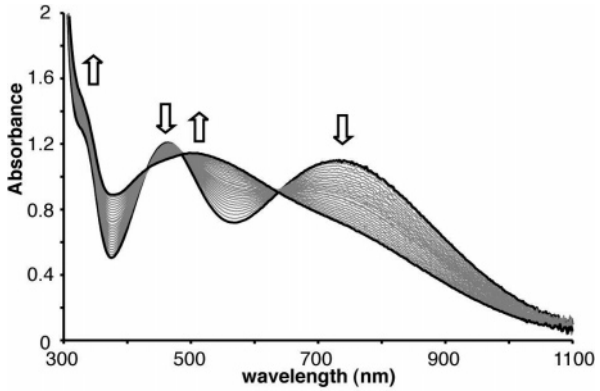

Figure 8. UV−vis spectral changes upon mixing $Fe(NO_3)_3 \cdot 9H_2O$, H**L4**, H_2dtbc, and 3 equiv of Et_3N in deoxygenated methanol. Arrows indicate the decrease or increase in absorption over time.

6 exhibits bands at 316, 524, and 720(sh) nm. The additional catecholato ligand in **6** is expected to give rise to two new catecholato-to-iron ligand-to-metal charge transfer (LMCT) transitions, the position of which is very dependent on the Lewis acidity of the ferric metal center.[20] The catecholato-to-iron LMCT bands in **6** overlap with the ligand LMCT transition, which results in the observed broad absorption feature.[57]

This overlap of LMCT bands can be nicely illustrated by monitoring the formation of the complex in time by UV−vis spectroscopy. When $Fe(NO_3)_3 \cdot 9H_2O$, H**L4**, H_2dtbc, and 3 equiv of Et_3N are mixed together at room temperature under anaerobic conditions, first a greenish solution is obtained, which gradually turns purple. The changes in the UV−vis absorption spectra are displayed in Figure 8.

Initially, two bands are observed at 460 and 730 nm. These bands can be assigned to catecholato-to-iron(III) charge-transfer transitions. The characteristic phenolato-to-iron charge-transfer band is not yet present. In time, the intensity of the two original LMCT bands decreases and a new absorption around 510 nm grows in, signifying the slow coordination of the phenolato O-donor to the metal center. Finally, after 2 h, the solution turns purple and the absorption spectrum of independently synthesized **6** is obtained. One has to note that when H**L4** and the iron(III) salt are premixed,

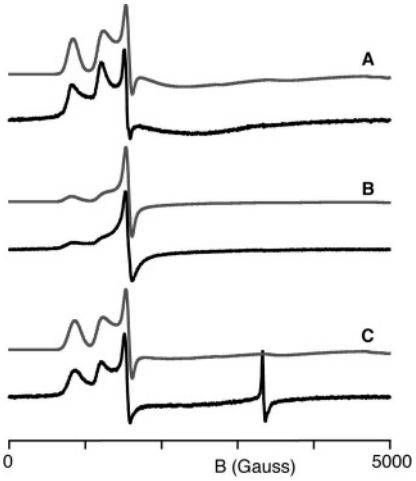

Figure 9. Simulated (gray) and experimental (black) X-band EPR spectra of 2 mM **4** (A), **5** (B), and **6** (C) solutions recorded in frozen methanol at 15 K. Typical EPR measuring conditions: microwave frequency 9.41 GHz, microwave power 0.5 mW, modulation amplitude 12.5 G, modulation frequency 100 kHz, and sweep width 5000 G. See Table 5 and the text for simulation parameters.

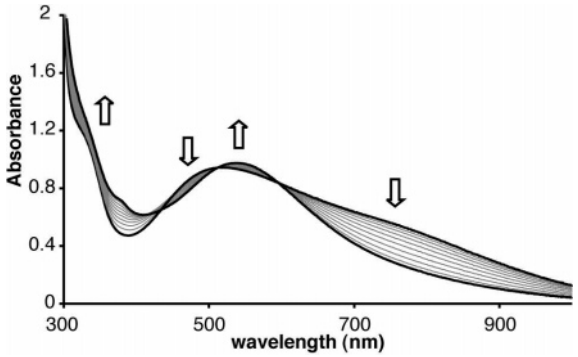

Figure 10. UV−vis spectral changes upon exposure of **6** in methanol to air. A spectrum was recorded every 20 min. Arrows indicate the increase or decrease in absorption over time.

as in the actual synthesis of **5** and **6**, the formation of this greenish species is not observed after the addition of the catechol. The blue solution immediately turns purple in this case.

Overall, the absorption spectrum of **6** shows a striking similarity to the absorption spectrum reported for the enzyme−substrate complex of protocatechuate 3,4-dioxygenase.[58] The E−S complex also features the broad tail on the phenolato-to-iron LMCT absorption with comparable extinction coefficients.

The dominant feature in the absorption spectra of **5** and **6** is the phenolato-to-iron charge-transfer band at 560 and 524 nm, respectively (Table 5). Que et al. showed that the phenolato-to-iron charge-transfer band reflects the strength of the other ligands coordinated to the iron. A weaker ligand would result in a stronger phenolato−iron interaction and a red-shift in the absorption maximum. The relative blue-shift of the absorption maximum upon going from a tetrachlorocatecholato ligand to the 3,5-di-*tert*-butylcatecholato ligand thus reflects the stronger interaction of the metal with the

(57) Que, L., Jr.; Kolanczyk, R. C.; White, L. S. *J. Am. Chem. Soc.* **1987**, *109*, 5373−5380.

(58) Bull, C.; Ballou, D. P.; Otsuka, S. *J. Biol. Chem.* **1981**, *256*, 12681−12686.

Table 5. Absorption Maxima in the UV−vis Spectra (λ_{max}, (ϵ (M^{-1} cm^{-1}))) and EPR Data[a] of the Complexes **4**−**6**

complex	λ_{max} (nm)	ϵ (M^{-1} cm^{-1})	$\eta = E/D$	$\Delta\eta$ (%)	g
$[Fe^{III}(\mathbf{L4})_2](NO_3)]$ (**4**)	318, 540	5400, 6400	0.12	15.5	8.3, 5.6
$[Fe^{III}(\mathbf{L4})(tcc)]$ (**5**)	303, 560	8500, 4000	0.15	20	8.7, 5.4
$[Fe^{III}(\mathbf{L4})(dtbc)]$ (**6**)[b]	316, 524, 720(sh)	5400, 4000, 2500	0.11	18	8.2, 5.6

[a] EPR spectra were recorded on 2 mM complex solution in frozen methanol at 15 K. [b] A minor low-spin Fe(III) species is also observed accounting for <1% of the total spin concentration.

latter ligand. Furthermore, the lower energy catecholato-to-iron LMCT transition is known to shift to higher energy as the substituents on the catechol ring are varied from electron donating to electron withdrawing, since electron-withdrawing groups would be expected to lower the energy of the catecholate frontier orbitals and thus increase the ligand-to-metal energy gap. In addition to this blue-shift of the catecholato-to-iron LMCT transitions and the red-shift of the ligand-to-iron LMCT transition, symmetry differences between the two catechols, i.e., non-two-fold symmetric dtbc catecholate and symmetric tcc could account for the less broad absorption spectrum that is observed for **5**.

Complexes **4**−**6** exhibit EPR spectra that show that these complexes are all high-spin ferric complexes (data given in Table 5). The EPR spectra of **4**−**6** are depicted in Figure 9; simulations are also included based on the standard spin Hamiltonian

$$H_S = D[S_z^2 - S(S+1)/3] + E(S_x^2 - S_y^2) + g\beta \mathbf{B}\cdot\mathbf{S}$$

and on the assumption of the weak-field limit, $D \gg h\upsilon$. In general, the spectra of distributed high-spin transition ion complexes are frequently found to be rather broad, presumably reflecting a distribution in electronic structure as a consequence of the relative geometrical flexibility of the complex. This leads to a distribution in the zero-field splitting (ZFS) parameters, which has been named *D* strain.[59] The resulting EPR spectra can be simulated by summing a large number of spectra calculated for different ZFS values.[60] However, our multifrequency EPR studies of $S = {}^5/_2$ models and metalloproteins have pointed to the difficulty of establishing the quantitative nature of their ZFS distributions.[60−62] Recently, Weisser et al. have presented an analysis of the EPR spectra of iron−catecholato complexes by simulation as ZFS-distributed $S = {}^5/_2$ systems.[63] An unexpected result of this study was the conclusion that a $g = 4.3$ signal commonly present in the spectra is not an $S = {}^5/_2$ contaminant of high rhombicity ($E/D \approx {}^1/_3$) but rather is an intrinsic part of the iron catecholato spectrum whose ZFS distribution is very broad to the extent that even extreme values of rhombicity are sampled with finite intensity by the distribution.[63] This is an attractive proposal because it resolves the apparent problem of a contaminating spectral component in chemically pure compounds. On the other hand, the analysis of Weisser et al. used a detailed distribution model with seven adjustable parameters including the absolute value of the axial ZFS parameter, *D*, while it has thus far been generally taken to be impossible to determine the value of *D* from data recorded at a single X-band frequency and a single temperature for systems near the weak-field limit (cf. ref 64).

We have, therefore, attempted to fit the present data with a drastically simplified model of only two parameters: the absolute values of *D* and *E* are undetermined; only the rhombicity $\eta = E/D$ is a fitting parameter (i.e., the weak-field limit[64]). Also, the Gaussian distributions in *D* and *E* are assumed to be fully correlated, and their standard deviations are identical when expressed as a percentage of the ZFS values; this gives a second fitting parameter, $\Delta\eta$ (cf. Table 5). Because the high-spin Fe^{III} d^5 system is subject to quenching of orbital angular momentum, it is assumed that the real *g* value does not significantly deviate from the free-electron value, $g = 2.00$. In Figure 9, it can be seen that this simple model affords semiquantitative fits to the data and, notably, corroborates the proposal[63] that the $g = 4.3$ line is an intrinsic part of the EPR spectrum of iron compounds of intermediate rhombicity subject to a broad distribution in rhombicity.

The EPR powder spectrum of **4** shows features at $g = 8.3$ and 5.6 and a broad feature at $g \approx 3$. The fitted rhombicity, $\eta = 0.12$, defines the effective g_{zyx} values of the three transitions within the Kramers doublets to be (1.60, 8.32, 3.25), (5.57, 2.41, 2.65), and (9.97, 0.09, 0.10) for the lowest, middle, and highest doublet, respectively. Thus, one observes the g_y of the lowest doublet, the g_z of the middle doublet, and a broad feature from a combination of the g_x of the lowest doublet and the g_y and g_x of the middle doublet. The other effective *g* values are associated with features that are beyond detection due to low intensity, broadening, or magnetic field limitation. And the $g = 4.3$ feature is from a small subset of molecules with maximally rhombic coordination sites that happen to be subject to extensive *D* strain.

In the spectrum of **6**, a minor feature is observed around $g \approx 2$, which is not accounted for by the distributed $S = {}^5/_2$ simulation. The signal is possibly attributable to a minority low-spin Fe(III) species; its integrated intensity accounts for <1% of the total spin concentration.

There is a marked similarity between the EPR spectra of **4**−**6** among themselves and also compared with other reported EPR spectra of iron(III)−catecholato complexes.[20,31,63] Especially, a comparison of the spectral data of the six-

(59) Hagen, W. R. *J. Magn. Reson.* **1981**, *44*, 447−469.
(60) Hagen, W. R.; Dunham, W. R.; Sands, R. H.; Shaw, R. W.; Beinert, H. *Biochim. Biophys. Acta* **1984**, *765*, 399−402.
(61) Priem, A. Explorations in High Frequency EPR. Ph.D. Thesis, Nijmegen University, The Netherlands 2002.
(62) Priem, A.; van Bentum, P. J. M.; Hagen, W. R.; Reijerse, E. J. *Appl. Magn. Reson.* **2001**, *21*, 535−548.
(63) Weissner, J. T.; Nilges, M. J.; Sever, M. J.; Wilker, J. J. *Inorg. Chem.* **2006**, *45*, 7736−7747.
(64) Hagen, W. R. *Dalton Trans.* **2006**, 4415−4434.

Table 6. Organic Products Obtained upon Reaction of Complex **6** with Air

solvent	additive	conv (%)	extradiol (%)	intradiol (%)	quinone (%)
MeCN		62	49 (61/39)[a]	40	11
CH_2Cl_2		58	51 (61/39)	41	8

[a] Ratio in parentheses: (4,6-di-*tert*-butyl-2-pyrone/3,5-di-*tert*-butyl-2-pyrone).

coordinated iron(III)−catecholato complexes **4** and $[Fe^{III}(hda)(dtbc)]^{2-}$ ($E/D = 0.15$) (hda = *N*-(2-hydroxybenzyl)-*N*-(carboxymethyl)glycine)[20] and **6** suggests that the latter is probably also six-coordinate in solution. A solvent molecule is then assumed to occupy the sixth available site, as also observed in the crystal structure of **5**·H_2O (vide supra).

Dioxygen Reactivity. Upon the exposure of **6** to air, a slow and subtle color change was observed. This process was monitored by UV−vis absorption spectroscopy, and in time, the broad absorption feature disappeared and concomitantly a new feature appeared with an absorption maximum at 536 nm (Figure 10). No changes were observed in the absorption spectra of **4** or **5** upon exposure to air. The loss in absorption intensity at longer wavelengths, originally attributed to the lower-energy catecholato-to-iron LMCT transition, suggested oxidative transformation of the catechol in the case of **6**. The new band that emerged at 550 nm can be ascribed to a $[Fe^{III}(\mathbf{L4})_2]^+$ species, given the similarity with the absorption spectrum of **4**. The $[Fe^{III}(\mathbf{L4})_2]^+$ species can account for only half of the total amount of iron present in solution, while other iron complexes may also form. Indeed, only two out of the three isosbestic points observed in Figure 10 are well-defined, indicating more than two principal species and the involvement of other species in the oxygenation reaction.

In order to identify the products and the regioselectivity of the reaction, the products were isolated from the reaction mixture, characterized by ^{1}H NMR spectroscopy and GC-MS, and compared to authentic samples. The oxygenation reactions were performed in both coordinating and noncoordinating solvents, i.e., acetonitrile and dichloromethane. A similar product distribution was found for the oxygenation reactions in the two different solvents (Table 6). In general, the reactions proceeded slowly, and after two weeks only about 60% of the catechol was converted. Both intradiol-*and* extradiol-type cleavage products were observed in a roughly equal ratio for both solvents, with a slight preference for the extradiol-type cleavage product. The amount of detected quinone auto-oxidation product is rather low.

Discussion

The intricacies of the respective regioselectivities of the intra- and extradiol-cleaving catechol dioxygenases are not yet completely understood and are the subject of ongoing research.[2−4] Many *functional* models of the intradiol-cleaving dioxygenases have been reported,[3,10,14,17−19,21,24,25,27,65] among which the tpa-derived complexes feature prominently.[15,16,22,66] Small synthetic analogues that accurately mimic the *structural* features of the active site of the intradiol-cleaving enzymes are, however, more limited in number. The best structural and spectroscopic model for the as-isolated $His_2Tyr_2Fe^{III}OH$ state of the intradiol-cleaving enzymes is the $[Fe(Mes_6\text{-salen})(H_2O)](ClO_4)$ complex reported by Fujii et al.[67,68] We anticipated that **L4**[33] could be an attractive candidate for obtaining a close structural mimic of the His_2-TyrFeCat state of the enzyme−substrate complex. Since no metal complexes of **L4** were reported to date, the facial-capping potential of **L4** was first explored by the synthesis of the 2:1 ligand-to-metal complex **4**. The crystal structure of **4** shows that the ligand can indeed act as a tridentate, facially coordinating ligand, rendering it a good mimic of the His_2Tyr facial triad.

The iron(III)−catecholato complexes **5** and **6** of ligand H**L4** are originally isolated as five-coordinate complexes. The structural data shows that a sixth coordination site is available and readily accessible for the coordination of small molecules like water. The availability of an empty coordination site is important, since it is one of the essential features of the E−S complex. Complexes **5** and **6** are directly related to the previously reported $[Fe^{III}(\mathbf{L1}-\mathbf{L3})(tcc)]$ and $[Fe^{III}(\mathbf{L1}-\mathbf{L3})(dtbc)]$ complexes[31] and differ only in the type of oxygen donor offered by the ligand (Chart 1). The influence of the ligand donor set on the dioxygenase reactivity of a ferric metal center can now be directly probed by comparison of the two types of complexes.

The X-ray structure of **5**·H_2O and the spectroscopic data of **5** and **6** show that the iron−catecholato complexes not only duplicate the structural features of the active site of the E−S complex of the intradiol-cleaving catechol dioxygenases but also closely resemble its spectral characteristics.[4,58] $[Fe^{III}(\mathbf{L4})(tcc)(H_2O)]$ (**5**·H_2O) is actually the closest, crystallographically characterized structural model of the E−S complex of the intradiol-cleaving enzymes reported to date. The oxidative cleavage of the catechol upon exposure of complex **6** to air was found to proceed slowly and with only moderate conversions (around 60%). The slow reactivity can be ascribed to the low Lewis acidity of the iron(III) metal center[21,22] compared with complexes with neutral, all-N ligands and was observed before for complexes with phenolato groups in the ligand set.[29,57]

The low Lewis acidity can, however, only be part of the answer, since the enzyme manages to show good turnover ($\approx$36 s^{-1} for 3,4-PCD with the product release as rate-limiting step)[4] with the same donor set. In the enzyme, the combination of hydrogen-bonding interactions with second-sphere residues and the precise positioning of the substrate in the binding pocket results in an enhanced asymmetric binding of the substrate. The asymmetric binding of the ligand enhances the iron(II)−semiquinonato character. This

(65) Koch, W. O.; Krüger, H.-J. *Angew. Chem., Int. Ed.* **1995**, *34*, 2671−2674.

(66) Higuchi, M.; Hitomi, Y.; Minami, H.; Tanaka, T.; Funabiki, T. *Inorg. Chem.* **2005**, *44*, 8810−8821.

(67) Fujii, H.; Funahashi, Y. *Angew. Chem., Int. Ed.* **2002**, *41*, 3638−3641.

(68) Kurahashi, T.; Oda, K.; Sugimoto, M.; Ogura, T.; Fujii, H. *Inorg. Chem.* **2006**, *45*, 7709−7721.

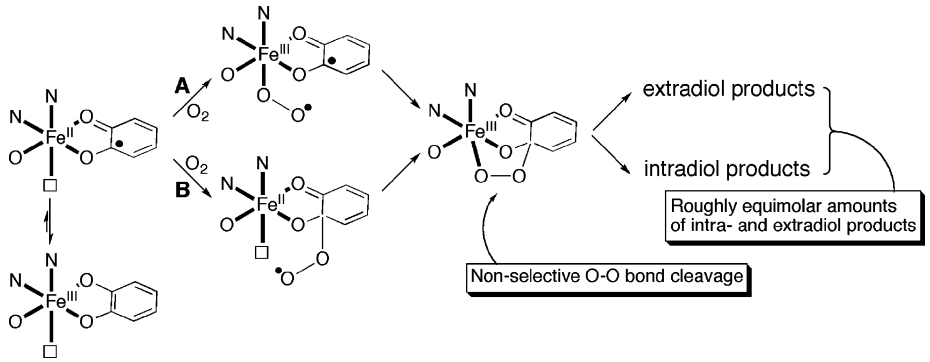

Figure 11. Proposed oxidative cleavage mechanism for **6**.

(increased) radical character is thought to be essential for dioxygen reactivity[3,12] and is further stabilized by the local dielectric properties of the enzyme active site. The combination of these factors lead to a lower activation barrier and comparably high catalytic activity of the natural systems.

Despite the rather low reactivity, important observations can be made regarding the selectivity of the oxygenation reaction. The product distribution is remarkably less solvent dependent than that previously observed for the extradiol model complexes [Fe^{III}(**L1**−**L3**)(tcc)]. The oxygenation of **6** in acetonitrile results in 90% oxidative cleavage products with only 10% quinone formation, whereas quinone was the only product observed for the oxygenation of [Fe^{III}(**L1**−**L3**)-(tcc)] in acetonitrile. Interestingly, both intradiol- *and* extradiol-cleavage products are formed in more or less equal amounts. The product distribution for the oxygenative cleavage of **6** thus shows that there is no inherent preference for intra- or extradiol-type cleavage by an iron(III) metal center coordinated by a N_{im},N_{im},O_{phen}-donor set. The same conclusion was drawn for the oxygenative cleavage in [Fe^{III}-(**L1**−**L3**)(dtbc)]. This illustrates that in both cases the endogenous ligand donor set in the enzyme is not a decisive factor for the regioselectivity of the cleavage. These results support the hypothesis that both the intradiol- and extradiol-cleaving enzymes proceed through a similar intermediate, i.e., a bridged alkylperoxo species, albeit with different iron oxidation states (Figure 11).

Such an intermediate is accessible in both complexes reported here and in our previous study. The oxygenative cleavage of **6** is initiated by the introduction of some iron(II)−semiquinonato character on the complex as indicated by the catecholato-to-iron(III) charge-transfer transitions.[10] As a consequence of the tripodal, tridentate nature of the ligand, an empty coordination site is available trans to the 1-methylimidazole donor groups that mimics His224 in the active site of the enzyme. The bridged alkylperoxo species can then be formed by either binding of dioxygen to the metal center at the vacant site and subsequent attack of the semiquinone by a superoxide species (Figure 11, A) or alternatively by direct attack on the substrate and subsequent recombination with the metal center at the vacant site (Figure 11, B).[3,12] The latter pathway has been preferred based on the available spectroscopic data,[3] but recent hybrid DFT calculations suggest that this is unlikely and rather point to pathway A.[12] The available data does not allow us to distinguish between the two possible pathways in the case of **6**. Finally, the nonselective cleavage of the O−O bond of the alkylperoxo species leads to roughly equal amounts of intra- and extradiol-type cleavage for complex **6**.

Conclusions

In addition to our reported mimics of the extradiol-cleaving catechol dioxygenases, we have studied the iron(III) coordination chemistry of the tripodal, tridentate ligand H**L4**, as a potential mimic of the endogenous ligands of the intradiol-cleaving catechol dioxygenases. The structurally characterized iron−catecholato complex [Fe^{III}(**L4**)(tcc)(H_2O)] can be regarded as the closest structural model of the enzyme−substrate complex reported to date. As part of its spectroscopic characterization, the EPR spectra were successfully simulated using a simplified model that accounts for *D* strain. The simulation procedure showed that the $g = 4.3$ line is an intrinsic part of the EPR envelope of the studied complexes and should not necessarily be attributed to a highly rhombic impurity. Oxygenation studies of the complexes revealed that equal amounts of intradiol- and extradiol-type cleavage products are formed. This suggests that the first coordination sphere of the metal center at the enzyme active site is not decisive for regioselective intradiol cleavage.

Addendum. Recent crystallographic studies by Kovaleva and Lipscomb on homoprotocatechuate 2,3-dioxygenase, an extradiol-cleaving catechol dioxygenase, have shown the formation of a side-on Fe-bound dioxygen species (Kovaleva, E.G.; Lipscomb, J.D. *Science* **2007**, *316*, 453−457). Such a side-on bound species may also be of relevance to the mechanism of operation of the intradiol-cleaving dioxygenases.

Acknowledgment. This work was financially supported by the National Research School Combination-Catalysis (P.C.A.B.) and the Council for Chemical Sciences of The Netherlands Organization for Scientific Research (CW-NWO) (M.L. and A.L.S.).

Supporting Information Available: CIF file of crystal data collection and refinement parameters, atomic coordinates, bond lengths and angles, anisotropic displacement parameters for compounds H**L4**, **4**, and **5**·H_2O. This material is available free of charge via the Internet at http://pubs.acs.org.

IC700741V